Research Article | Vol. 28, No. 23 / 9 November 2020 / Optics Express 34574
Optics EXPRESS

Thin-disk laser-pumped OPCPA system delivering 4.4 TW few-cycle pulses

MARTIN KRETSCHMAR,[1,*] JOHANNES TUEMMLER,[1] BERND SCHÜTTE,[1] ANDREAS HOFFMANN,[1] BJÖRN SENFFTLEBEN,[1] MARK MERO,[1] MARIO SAUPPE,[1,2] DANIELA RUPP,[1,2] MARC J. J. VRAKKING,[1] INGO WILL,[1] AND TAMAS NAGY[1]

[1]*Max Born Institute for Nonlinear Optics and Short Pulse Spectroscopy, Max-Born-Str. 2A, 12489 Berlin, Germany*
[2]*ETH Zürich, John-von-Neumann-Weg 9, 8093 Zürich, Switzerland*
[*]*Martin.Kretschmar@mbi-berlin.de*

Abstract: We present an optical parametric chirped pulse amplification (OPCPA) system delivering 4.4 TW pulses centered at 810 nm with a sub-9 fs duration and a carrier-envelope phase stability of 350 mrad. The OPCPA setup pumped by sub-10 ps pulses from two Yb:YAG thin-disk lasers at 100 Hz repetition rate is optimized for a high conversion-efficiency. The terawatt pulses of the OPCPA are utilized for generating intense extreme ultraviolet (XUV) pulses by high-order harmonic generation, achieving XUV pulse energies approaching the microjoule level.

© 2020 Optical Society of America under the terms of the OSA Open Access Publishing Agreement

1. Introduction

Most laboratory-based time-resolved spectroscopy studies in the extreme ultraviolet (XUV) spectral region utilize a pair of infrared and XUV pulses for pumping and probing processes on ultrashort timescales [1–4]. Nowadays a few research groups pursue the application of few-femtosecond (fs) to attosecond (as) XUV pulses for both pumping and probing [5,6]. For this purpose up-scaling of the XUV pulse energy is necessary, requiring TW-level few-cycle pulses to drive the frequency conversion process of high-order harmonic generation (HHG) [7–9]. Besides post-compression of laser pulses in large hollow-core fibers [10–12], optical parametric chirped pulse amplification (OPCPA) is well suited for the generation of these high-energy driving pulses [13,14].

The optical parametric amplification (OPA) scheme enables the direct amplification of few-cycle pulses, due to the large phase-matching bandwidth of the underlying second-order nonlinear process [15]. This technology enables the construction of multi-TW, few-cycle systems capable of generating relativistic intensities [16,17]. The generation of the required high-energy pump beams for the OPA process often relies on neodymium-based amplifier systems. Due to superfluorescence during pumping, significant temporal pedestals can arise, which can be detrimental in a number of high-intensity experiments. To improve the pre-pulse temporal contrast, picosecond Nd:YAG pump lasers have been employed with durations between 60 ps - 80 ps [14,16–18]. However, even such ps Nd:YAG-laser-pumped systems can exhibit a 10-30 ps long non-negligible pedestal preceding the main pulse [16,18], that may lead to unwanted modification of the target before the main pulse arrives e.g. in relativistic surface HHG [19]. In order to decrease the energy deposition prior to the main pulse one can utilize ytterbium-based amplifiers for pumping which can provide significantly shorter pump pulses with a duration on the order of 1 ps to confine the background radiation to that narrower time window [20,21]. However, this advantage comes at a high price, as shorter pump pulses introduce a number of technical problems which can considerably influence the architecture and performance of such systems. By decreasing the pulse duration, it becomes more difficult to keep the nonlinear phase distortions of the pump and

#404077 https://doi.org/10.1364/OE.404077
Journal © 2020 Received 29 Jul 2020; revised 6 Oct 2020; accepted 7 Oct 2020; published 29 Oct 2020

Optics EXPRESS

signal beams at a tolerable level [22]. At sub-ps pump pulse duration the compression of the pump pulses and the full parametric amplification chain need to be located in vacuum in order to suppress unwanted nonlinearities [20]. Furthermore, few-ps pumped high energy OPCPA systems are known to be sensitive to the alignment of the relative pulse fronts of pump and signal beams, where a mismatch results in a deterioration of the achievable conversion efficiency, the output beam profile as well as the spatio-temporal characteristics of the signal beam [20,22].

In this paper, we demonstrate a 100 Hz OPCPA that is pumped by two high-energy Yb:YAG thin-disk lasers delivering carrier-envelope phase (CEP) stable pulses with a duration of 8.3 fs and an energy of 42 mJ with excellent long-term stability. By using pump pulses with an intermediate duration of ≤5.5 ps we generate high-contrast 4.4 TW pulses with a pre-pulse region confined to 2.9 ps at a record efficiency of more than 30% without significant spatio-temporal distortions. To our knowledge this is the first thin-disk-pumped OPCPA delivering above-TW few-cycle pulses.

The system is part of a new extreme-ultraviolet beamline at the Max Born Institute in Berlin aiming at the generation of high XUV peak intensities [23]. In a first experiment, the intense few-cycle pulses are applied for HHG in xenon resulting in XUV pulses with an energy at the μJ-level.

2. System layout and experimental results

Before describing the design of the OPCPA and its pump lasers in detail, we provide a brief overview of the system. The layout of our OPCPA system is depicted in Fig. 1. A Yb:KGW-driven frontend (Light Conversion Ltd.) [24] provides the seed pulses for the pump and provides, following white light generation, optically synchronized signal pulses for the three consecutive OPCPA stages.

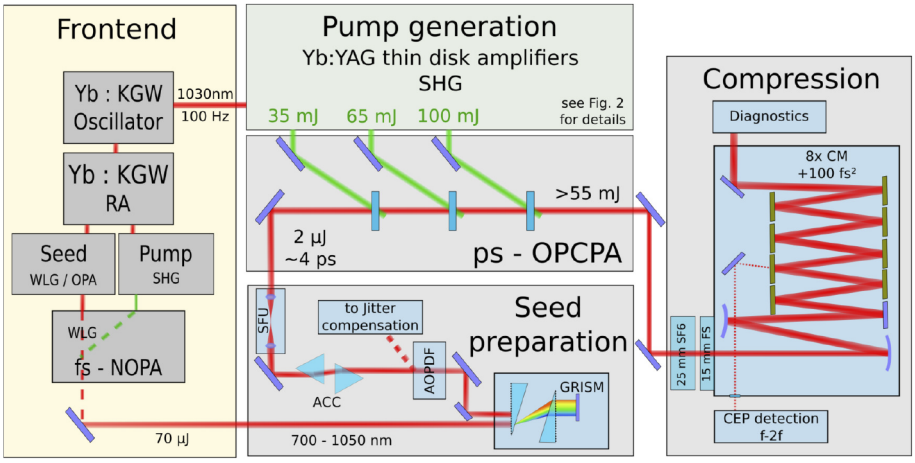

Fig. 1. Schematics of the OPCPA architecture. WLG: white-light generation, SFU: spatial filtering unit, SCC: spatial-chirp compensation, CM: chirped mirror.

A fraction of the oscillator's output seeds two Yb:YAG thin-disk amplifiers, which provide the pump pulses (see section 2.1). The ytterbium-doped amplifiers deliver high-energy pulses with a transform-limited duration of 1.6 ps, which is advantageous for achieving large contrast. However, a number of issues arise if the OPCPA pump pulses are very short and hence their peak power is high: First, in order to obtain high stability of both the pulse energy and the CEP of the signal pulses amplified in the OPCPA, the timing jitter between the pump and seed should be significantly smaller than the pump pulse duration. The shorter the pulses are the more stringent this becomes. Second, in order to keep the intensity of both the pump and the

Optics EXPRESS

amplified seed pulses below the damage threshold, a decrease of the pump pulse duration implies that the beam size on the nonlinear crystal should increase. However, the possibility to do so is limited by the maximum available crystal size of 25 mm in case of beta-barium borate (BBO), which is our crystal of choice. Third, the spatial beam quality of the pump pulses has a big influence on the efficiency of the parametric process as well as on the beam quality of the amplified pulses. Therefore, excessive intensity-dependent nonlinear phase modulation of the pump pulses accumulated during propagation (B-integral) in atmosphere and in the OPA crystals has to be prevented, as it leads to significant degradation of the beam quality or even to beam break-up [22]. We find a good trade-off between all these considerations for a pump pulse duration of 5 ps, which brings the pump intensity in the BBO crystals below the estimated damage threshold of 75 GW/cm^2 and the B-integral accumulated along the necessary 4 m air propagation to an acceptable level of 0.7 rad. Consequently, we use the ≈5 ps long second harmonic of the positively chirped Yb:YAG pulses centered at 515 nm for pumping the three subsequent OPA stages at energies of 35 mJ, 65 mJ and 100 mJ, respectively.

The main part of the frontend generates broadband, passively CEP-stabilized seed pulses with an rms CEP stability <250 mrad and a spectrum spanning from 700 to 1050 nm via a cascade of white light and difference frequency generation stages. Two subsequent parametric pre-amplifiers pumped by the frequency-doubled output of the Yb:KGW regenerative amplifier bring the pulse energy to 70 μJ [24].

Before the main amplification can take place, a GRISM-stretcher in combination with an acousto-optical programmable dispersive filter (Dazzler) [25] negatively chirps the seed pulses to ≈4 ps duration. A prism pair is utilized to compensate the spatial chirp induced by the Dazzler, and a subsequent spatial filter ensures that the seed beam of the parametric amplification is free of spatial inhomogeneities. Owing to the large losses introduced by the DAZZLER and the GRISM, the seed pulse energy is reduced to 2 μJ.

The stretched pulses are then amplified in a sequence of three picosecond OPA stages made of large-aperture (20 mm x 20 mm) BBO crystals to a pulse energy of 57 mJ, as detailed in section 2.2. The final pulse compression of the amplified picosecond pulses is achieved by a combination of positive material dispersion and positively chirped mirrors which is described in section 2.3.

2.1. High energy thin-disk pump lasers

Thanks to their geometry, thin-disk amplifiers feature an efficient cooling mechanism which supports operation at high average power up to the kW level [26,27]. Using broadband Yb-doped media, such amplifiers can deliver high-energy ps pulses which are well-suited for pumping OPCPA stages.

The generation of the high-energy pump pulses is sketched in Fig. 2. The seed pulses of the amplifier chain of the pump laser originate from the Yb:KGW oscillator in the frontend. They are picked at a repetition rate of 100 Hz by a Pockels cell and have an energy of less than 10 nJ within the amplification bandwidth. The pulses are temporally stretched to a duration of approximately 1 ns and subsequently boosted to an energy of 2 mJ in a dedicated regenerative Yb:KGW pre-amplifier. After pre-amplification, the pulses are split into two equal parts for seeding two parallel Yb:YAG thin-disk amplifier stages [28]. In contrast to [28,29], the amplifiers are seeded with a higher pulse-energy, which enables a reduction of the number of round trips and consequently leads to an improved energy stability. Figure 3 shows a measurement of the output energy of the two amplifiers, which is well beyond 200 mJ for both channels with an excellent stability of less than 0.5% rms. A pair of vacuum spatial filters relay the amplified pulses into two parallel grating compressors. The infrared pulses at 1030 nm with a Fourier limit of 1.6 ps are compressed to a pulse duration of ≈ 8 ps, as shown in Fig. 2, and further relay imaged towards the OPCPA stages with another set of vacuum spatial filters.

Optics EXPRESS

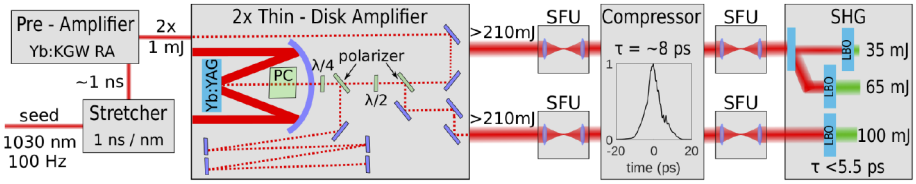

Fig. 2. Layout of the high-energy pump beam generation. RA - regenerative amplifier, PC - Pockels cell, SFU - spatial filtering unit and SHG - second-harmonic generation.

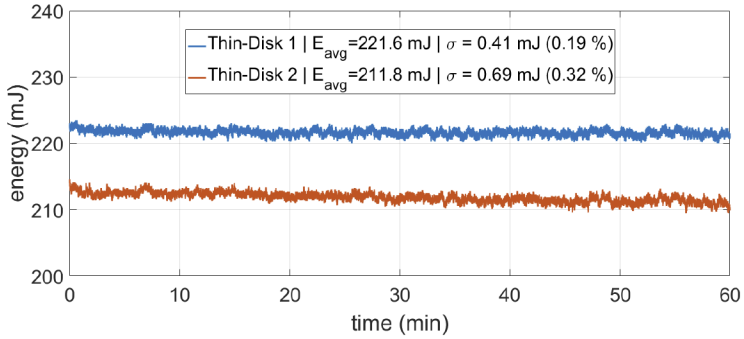

Fig. 3. Output energy of the two high-energy thin-disk regenerative amplifiers recorded over a period of one hour.

One of the pump arms is split into two with a polarization-sensitive splitter. This allows for adjusting the splitting ratio by rotating a half-waveplate to provide optimal pump energy for both the first and second parametric amplification stages. All three beams are frequency-doubled in 4 mm long LBO crystals, generating pump beams centered at a wavelength of 515 nm with estimated pulse durations of ≈ 5.5 ps for the first two and ≈ 4.5 ps for the third stage, respectively. The pump pulse duration was measured by a commercial second-order autocorrelator (PulseCheck, APE). The pump for the third stage is compressed to a slightly shorter duration in order to better match the signal pulses that become slightly compressed within the amplifier due to positive material dispersion in the first two OPA stages. In our system, the timing jitter between the seed and the pump pulses is actively stabilized. We use the non-refracted seed pulses from the DAZZLER which are highly chirped. In auxiliary OPA stages for each pump beam the strongly chirped signal is amplified by the pump pulses. As the timing between the pulses changes, the central wavelength of the amplified pulses shifts which is detected by a simple spectrometer [30] and coupled back to motorized delay stages placed in front of each of the two thin-disk amplifiers. In this way the temporal jitter after stabilization is reduced to $\approx$1% (26 fs and 56 fs for the two pump lasers, respectively) supporting good energy and CEP stability of the amplified pulses.

2.2. *Few-Picosecond Parametric Amplification*

The parametric amplification in a non-collinear geometry for broad phase-matching bandwidth is distributed over three consecutive stages, as shown in Fig. 1. The nonlinear medium of each stage is a 24.5°-cut BBO crystal in which the signal and pump beams cross each other at an angle of 2.45° according to the pointing-vector-walk-off-compensation (PVWC) geometry.

The parameters for each amplification stage are summarized in Table 1. In the first stage, the 2 μJ pulses of the signal beam with a diameter of 3 mm are amplified up to a level of 6 mJ by using a pump energy of 35 mJ. After passing the first stage, the beam is expanded by a factor of four to about 12 mm in order to match the size of the pump beams of the subsequent stages. The

Optics EXPRESS

second and third stage are driven into saturation with high pump-to-signal energy conversion efficiencies of ≈ 30% boosting the energy of the signal to 25 mJ and 57 mJ, respectively. Although we use nearly Gaussian pump beams, an exceptionally high conversion efficiency is achieved by applying high peak intensities in the nonlinear medium and tightly matching both the temporal and spatial profile of the pump and seed in the amplification stages. In our setup, the pump pulses are only 1.2-1.4 times longer than the seed pulses, which slightly reduces the bandwidth of the amplified signal. At the same time the diameter of the pump beams exceed the signal beam size by less than 25%. This tight matching ensures an optimal overlap between the pump and signal beams resulting in an efficient energy transfer. Furthermore, the conversion efficiency also benefits from the applied PVWC geometry because the idler is depleted through second-harmonic generation, resulting in a reduced back-conversion compared to the tangential phase-matching (TPM) configuration. Due to the large beam diameters of the pump and signal beams, we see no significant walk-off effects in either phase-matching configuration.

Table 1. Parameters of the three consecutive OPA stages. E: energy; I: intensity; σ: standard deviation of signal energy; l: length; $\eta_{P\text{-}S}$: conversion efficiency from pump to signal

Stage	E_{Pump} [mJ]	I_{Pump} [GW/cm^2]	E^{out}_{Signal} [mJ]	σ_{Signal} [%]	Gain	$l_{Crystal}$ [mm]	$\eta_{P\text{-}S}$ [%]
seed	-	-	0.002	-	-	-	-
1	35	65	6	0.99	3000	3	18
2	65	15	25.6	1.2	4.25	2	30
3	100	49.5	57.0	0.85	2.22	1.1	31
unseeded	-	-	0.55	13.6	-	-	-

Due to the similarly large beam diameters, and short pulse durations of the pump and signal, pulse-front matching in the non-collinear geometry may be necessary to ensure high conversion efficiency and beam quality. The pulse front of the pump pulses can be tilted by slightly misaligning the grating compressor in order to match those of the signal pulse [20]. At proper alignment, the amplified signal beam exhibits no significant spatial chirp, as no tilt is observable in Fig. 4(a), which shows the spatially-resolved spectrum of the signal pulse recorded at an energy of 55 mJ using a home-built imaging spectrometer. Furthermore, neither significant depletion nor back conversion can be seen in the spatially resolved spectrum. The strong spectral dip around 870 nm is a result of parasitic second-harmonic generation which is inherently present in the PVWC geometry. In order to further quantify the quality of the amplified picosecond beam, the beam profile was measured at several points along the caustics formed by a lens with a focal length of 3 m. Figure 4(b) shows from left to right the evolution of the beam profiles through the focus displaying no significant distortions in either the near or in the far field.

In order to find out how sensitive the parametric amplification is on the duration and on the pulse front tilt (PFT) of the pump pulses, the evolution of the signal energy inside the third BBO stage has been numerically modelled [31,32] using the pulse parameters of Table 1 (E_{pump} = 100 mJ, E_{signal} = 26 mJ). In the calculations two different pump pulse durations of 1 ps and 4.25 ps were considered, both with a matched and an unmatched PFT corresponding to the applied non-collinear angle of 2.45°. In each case the duration of the signal pulse was set to 70% of those of the pump pulse. In the simulations the beam diameter was set to 11 mm, corresponding to the experimental conditions in the third amplification stage. A space-time grid of 8192x8192 points with a box-size of 25 mm x 13.5 ps was used to model the parametric amplification. The findings, summarized in Fig. 5, show that pulse front matching is crucial for efficient parametric amplification in case of the 1 ps pulse, but plays a marginal role for the longer pulse. However, in case of PFT-matching, the output energy is 10% higher for the shorter pulse than for the

Optics EXPRESS

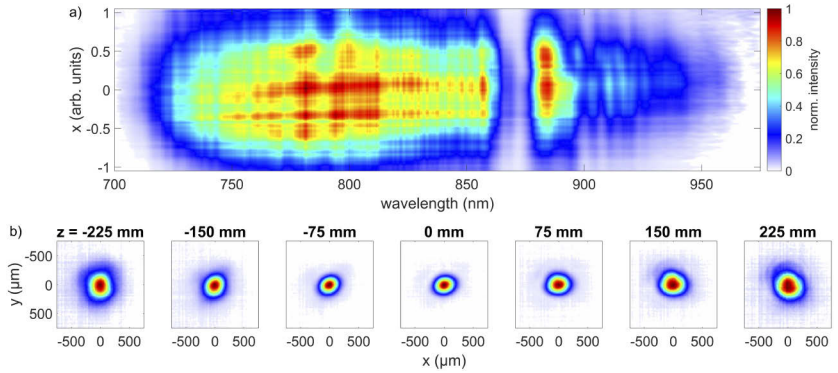

Fig. 4. Spatial characteristics of the amplified uncompressed beam. (a) spatially-resolved spectrum of the near-field beam and (b) the evolution of the beam along the caustics of a f=3 m lens.

4.25 ps pulse, showing that a higher pump intensity results in a higher conversion efficiency and a shorter optimal crystal length. We note that the accumulated nonlinear phase during parametric amplification up to the point of maximum energy conversion is 2.14x higher (0.28 rad compared to 0.13 rad) for the case of 1 ps pump pulses. These numerical findings show a reduced sensitivity to a PFT mismatch and reduced nonlinear distortions compared to the shorter pump pulses and elucidate the reason for the remarkably clean imaging spectrum and beam profiles (Fig. 4) measured after efficient parametric amplification.

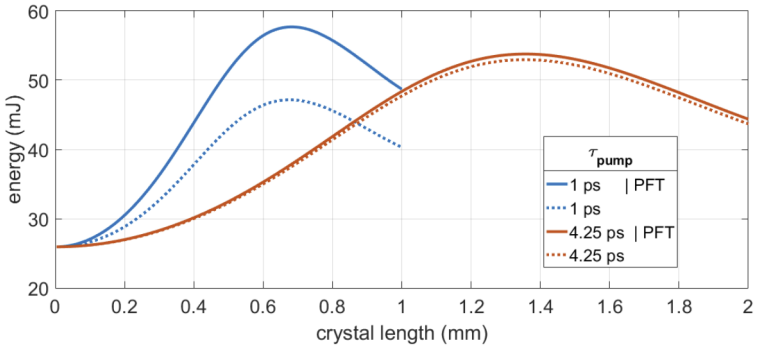

Fig. 5. Simulated pulse energy along the propagation in the OPA crystal for different pump pulse durations and for matched and unmatched pulse front tilt.

2.3. Temporal compression

The compression of the amplified pulses is performed by utilizing bulk material with positive dispersion in combination with eight positively chirped mirrors each having a nominal group delay dispersion (GDD) of +100 fs^2. The glass compressor unit consists of a 25 mm thick N-SF6 and a 15 mm thick fused silica substrate, whereas the latter also serves as the entrance window of a vacuum chamber where the final compression by the chirped mirrors takes place. To keep the B-integral along the glass material reasonably low, the beam is expanded to a diameter of approximately 60 mm (at $1/e^2$ level) before passing through the glass substrates and is subsequently reduced to a diameter of approximately 25 mm on the chirped mirrors. In this

Optics EXPRESS

way we keep the accumulated B-integral in the compression setup below 1.5 rad, preventing significant nonlinear distortion in the beam.

The compressed pulses are characterized by a non-collinear second-harmonic generation frequency-resolved optical gating setup (SHG-FROG). The measurement, displayed in Fig. 6, reveals a very clean pulse shape with duration of 8.3 fs full-width-at-half-maximum (FWHM). Achieving this pulse duration requires and relies on the precise dispersion control of the seed pulses by the DAZZLER. Furthermore, the PVWC geometry proves to be beneficial with respect to the pulse shape as the spectral form of the amplified pulses remains Gaussian-like resulting in clean, satellite-free transform-limited pulses opposed to common sinc-shaped pulses with pronounced satellites due to more square-cut spectra [14]. The main peak contains more than 90% of the energy and reaches a power level of 4.4 TW. The high-fidelity data reconstruction was performed on a grid size of 1024 points resulting in a FROG error of 0.25%.

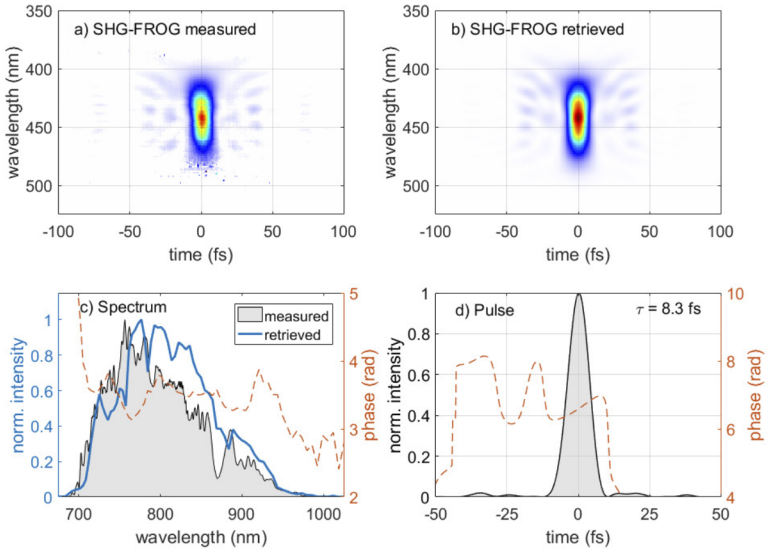

Fig. 6. SHG FROG measurement of the compressed pulses. The measured and retrieved traces are shown in a) and b), respectively. The measured and retrieved spectra are shown in c). The retrieved pulse shape, shown in d), has a duration of 8.3 fs (FWHM).

The CEP of the initial seed beam is passively stabilized as it is generated through difference frequency generation. In order to measure the CEP offset of the amplified pulses, the leakage through a chirped mirror is coupled out of the compression chamber. A home-made f-2f interferometer is used to measure the CEP. Exploiting amplitude-to-phase coupling in the WLG process, the output signal of the f-2f interferometer integrated over two laser shots is fed back to an attenuator in the seed WLG stage in the frontend. Thanks to the slow feedback loop we can obtain a CEP stability of 350 mrad for an extended periode of time, as shown in Fig. 7(a). This CEP stability is adequate for the attosecond science applications envisioned with the OPCPA system.

The pulse contrast is characterized on a 100 ps time scale using a long-range third-order autocorrelator (Sequoia, Amplitude Technologies). The measured trace shown in Fig. 7.b exhibits a clean pulse with high contrast solely limited by the noise floor of the autocorrelator at the level of 10^{-10}. The post-pulses (marked blue) of the trace can be associated to double reflections from 1 mm, 1.5 mm, 2 mm, and 3 mm thick optics, such as the BBO crystals of the OPA stages. There are also three pulses (also marked blue) observable prior to the main pulse which however, can be identified as ghosts of the three largest post-pulses, as they appear symmetrically to the main

Optics EXPRESS

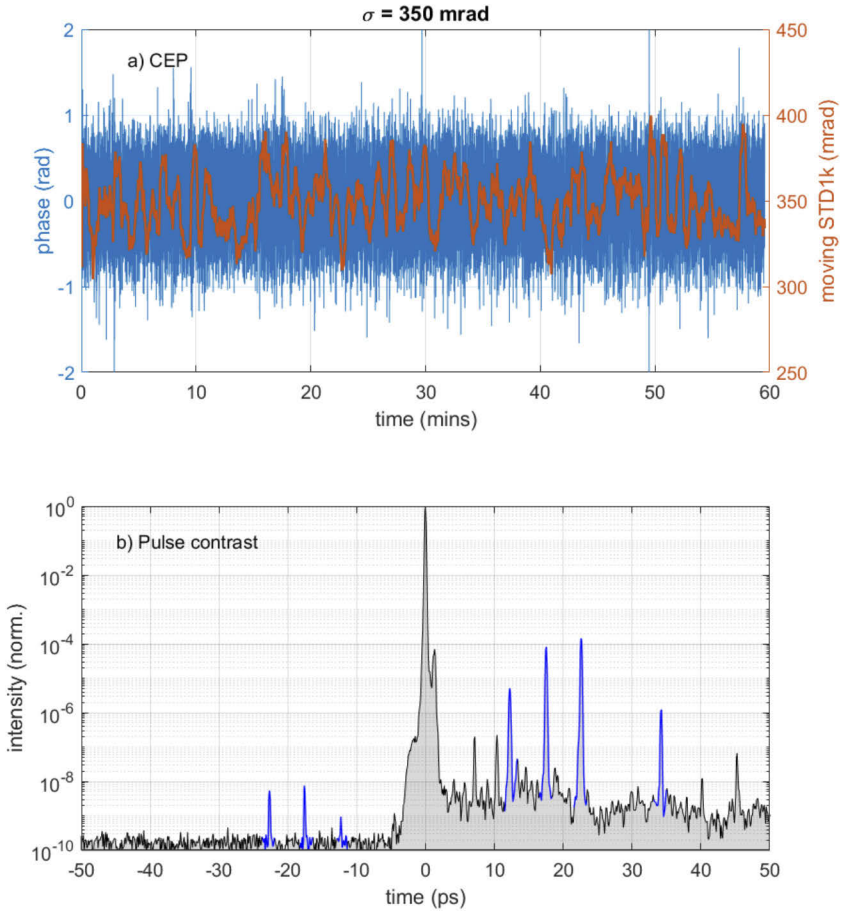

Fig. 7. (a) Carrier envelope phase measurement over a time span of one hour, showing an rms fluctuation of 350 mrad. The orange curve displays rms values calculated on a moving window of 1000 data points. (b) High-dynamic-range measurement of the pulse using a third-order autocorrelator. The three blue peaks before the main pulse are mirror images of those on the trailing side (see text for further details).

Optics EXPRESS

pulse and their intensity scales as the square root of these post pulses [20]. We note that the temporal resolution of the autocorrelator is about 50 fs which smears out the sub-9 fs main pulse in a greater extent than the less well-compressed sub-pulses or the much longer superfluorescence signal. Therefore, our measurement provides a lower limit of the pulse contrast performance. In comparison to [14] having a pre-pulse pedestal up to 6.5 ps preceding the main pulse, we were able to reduce the undesirable pre-pulse region to a tighter time window of 2.9 ps at a contrast level of 10^{-8} which is comparable to values obtained after extra contrast enhancement using a plasma mirror in another OPCPA pumped by long pump pulses [17].

The energy of the compressed pulses is recorded over one hour of operation. The measurement displayed in Fig. 8(a) shows an average value of 42 mJ and an excellent stability of 0.8% rms. An astigmatism-compensated reflective telescope consisting of a concave (R=-3 m) and a convex (R=2 m) silver mirror separated by 71.5 cm, is used to focus the amplified beam with an effective focal length of f = 7 m. The energy distribution of the focal spot is measured with a beam profiler (shown in Fig.7.b) exhibiting a round spot with a pedestal structure. The pedestals originate from higher-order aberrations of the large-aperture telescopes in the compressor. The focal diameter of d_0=465 μm at $1/e^2$ level is determined by fitting a Gaussian shape to the main peak containing 70% of the input energy. The peak intensity in the focus is estimated to be 3.6×10^{15} W/cm^2, enabling the straightforward application of the generated terawatt pulses in a wide range of strong-field experiments. With the implementation of an adaptive mirror for the correction of spatial aberrations we plan to further improve the focal properties of the beam and thus raise the peak intensity.

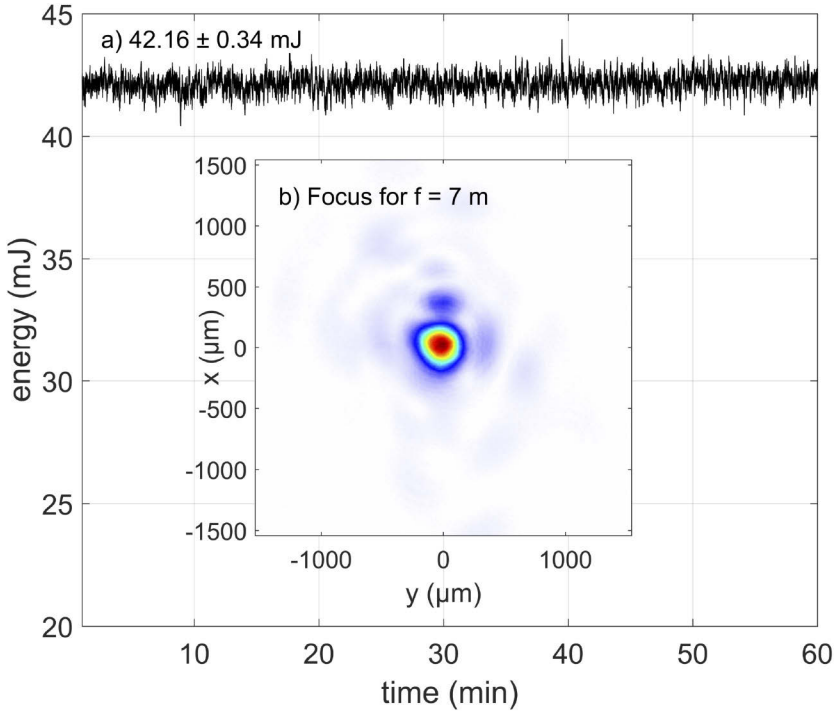

Fig. 8. (a) Energy of the compressed beam measured over a time of one hour. (b) Focal distribution of the output beam focused by a telescope of 7 m focal length.

Optics EXPRESS

3. High-order harmonic generation with terawatt pulses

The multi-TW, few-cycle near-infrared pulses are used for driving HHG in noble gases in order to obtain high-energy XUV-pulses. The loose focusing geometry of our reflective telescope supports a high generation yield by exciting a large number of emitters in the focal region. We use xenon gas in a 30 cm long gas cell at a pressure of ≈1 mbar as the generating medium. In the course of propagation through the cell the driver pulses, used in these preliminary experiments at a reduced energy of 10 mJ, undergo a spatio-temporal reshaping, which is beneficial for the phase matching and thus for the generation yield [33].

After generation, the harmonics freely propagate 12 m downstream in a vacuum beamline before getting tightly refocused. This asymmetrical arrangement using a large de-magnification of the HHG source maximizes the achievable intensity of the XUV pulses required in many pump-probe experiments [23]. Furthermore, the long distance ensures that the co-propagating infrared driving pulse is sufficiently expanded for putting a 100 nm thick aluminium filter into the beam. The filter completely blocks the infrared light and transmits the XUV radiation with a mean transmission of 40% for wavelengths <82 nm. At 100 Hz repetition rate we could maximize the throughput of our beamline by omitting mirror-based IR-suppression which is needed at kHz repetition rates e.g. in the high-XUV-flux beamlines at ELI-ALPS [13] and ELI Prague [34]. In this way we obtain a very high XUV intensity of up to $7\text{x}10^{14}$ W/cm^2, which enabled the observation of highly nonlinear ionization of Ar atoms [23]. The beam profile and spectrum of the generated harmonic radiation are recorded by an XUV spectrometer using the 0^{th} and 1^{st} diffraction order of an XUV-grating, respectively (see Fig. 9(a) and (b)). The XUV spectrum is clipped below the 11^{th} harmonic order by the aluminium filter and extends up to the 21^{st} harmonic. The XUV pulse energy is measured by an encapsulated XUV-diode shielded by an additional 100 nm thick aluminium filter with a transmission of 30% to reduce the influence of residual stray-light from the infrared beam. A lower estimate of the pulse energy is measured with a diode (AXUV from OptoDiode) to be 600 nJ in the given XUV spectral region, showing an rms stability of 2.25% over a time interval of 15 mins. The generated XUV radiation has already been applied to drive highly nonlinear ionization in noble gases [23] and we are currently working towards to use this XUV source for XUV-pump XUV-probe experiments [5] or single-shot coherent diffractive imaging experiments of isolated nanotargets [35] in the future.

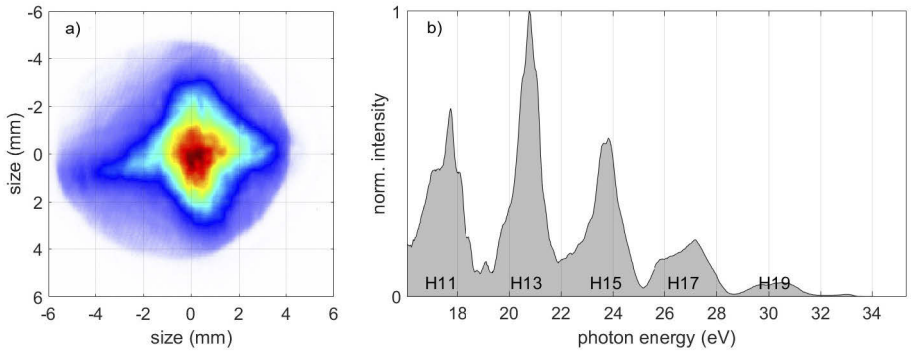

Fig. 9. XUV beam profile (a) and spectrum (b) from HHG in a 30 cm long gas cell filled with 1 mbar xenon.

4. Conclusion

In conclusion, we demonstrate an OPCPA system pumped by two high-energy Yb:YAG thin-disk lasers operating at a repetition rate of 100 Hz. To the best of our knowledge this is the first

Optics EXPRESS

thin-disk-pumped OPCPA system beyond the terawatt level. Thanks to the few-ps long pump pulses we achieve pump-to-signal energy conversion efficiencies in excess of 30% for the generation of 8.3 fs CEP-stable pulses with a peak power of 4.4 TW. The high contrast with a short pre-pulse region of less than 3 ps makes this source suitable for high-intensity applications. By focusing the pulses into a Xe-filled gas cell 600 nJ XUV pulses are achieved via high-harmonic generation. Therefore, we believe that with the new OPCPA we will be capable of performing XUV-pump XUV-probe experiments in the near future.

Acknowledgments

We thank G. Steinmeyer for his suggestions concerning the manuscript.

Disclosures

The authors declare no conflicts of interest.

References

1. M. Uiberacker, T. Uphues, M. Schultze, A. J. Verhoef, V. Yakovlev, M. F. Kling, J. Rauschenberger, N. M. Kabachnik, H. Schröder, M. Lezius, K. L. Kompa, H.-G. Muller, M. J. J. Vrakking, S. Hendel, U. Kleineberg, U. Heinzmann, M. Drescher, and F. Krausz, "Attosecond real-time observation of electron tunnelling in atoms," Nature **446**(7136), 627–632 (2007).
2. E. Goulielmakis, Z.-H. Loh, A. Wirth, R. Santra, N. Rohringer, V. S. Yakovlev, S. Zherebtsov, T. Pfeifer, A. M. Azzeer, M. F. Kling, S. R. Leone, and F. Krausz, "Real-time observation of valence electron motion," Nature **466**(7307), 739–743 (2010).
3. D. Azoury, M. Krüger, G. Orenstein, H. R. Larsson, S. Bauch, B. D. Bruner, and N. Dudovich, "Self-probing spectroscopy of xuv photo-ionization dynamics in atoms subjected to a strong-field environment," Nat. Commun. **8**(1), 1453 (2017).
4. M. Flögel, J. Durá, B. Schütte, M. Ivanov, A. Rouzée, and M. J. J. Vrakking, "Rabi oscillations in extreme ultraviolet ionization of atomic argon," Phys. Rev. A **95**(2), 021401 (2017).
5. P. Tzallas, E. Skantzakis, and D. Charalambidis, "Direct two-XUV-photon double ionization in xenon," J. Phys. B: At., Mol. Opt. Phys. **45**(7), 074007 (2012).
6. A. Peralta Conde, J. Kruse, O. Faucher, P. Tzallas, E. P. Benis, and D. Charalambidis, "Realization of time-resolved two-vacuum-ultraviolet-photon ionization," Phys. Rev. A **79**(6), 061405 (2009).
7. E. J. Takahashi, P. Lan, O. D. Mücke, Y. Nabekawa, and K. Midorikawa, "Attosecond nonlinear optics using gigawatt-scale isolated attosecond pulses," Nat. Commun. **4**(1), 2691 (2013).
8. G. Sansone, L. Poletto, and M. Nisoli, "High-energy attosecond light sources," Nat. Photonics **5**(11), 655–663 (2011).
9. F. Krausz and M. Ivanov, "Attosecond physics," Rev. Mod. Phys. **81**(1), 163–234 (2009).
10. S. Bohman, A. Suda, T. Kanai, S. Yamaguchi, and K. Midorikawa, "Generation of 5.0fs, 5.0mj pulses at 1khz using hollow-fiber pulse compression," Opt. Lett. **35**(11), 1887–1889 (2010).
11. T. Nagy, M. Kretschmar, M. J. J. Vrakking, and A. Rouzae, "Generation of above-terawatt 1.5-cycle visible pulses at 1khz by post-compression in a hollow fiber," Opt. Lett. **45**(12), 3313–3316 (2020).
12. M. Ouillé, A. Vernier, F. Böhle, M. Bocoum, A. Jullien, M. Lozano, J.-P. Rousseau, Z. Cheng, D. Gustas, A. Blumenstein, P. Simon, S. Haessler, J. Fauré, T. Nagy, and R. Lopez-Martens, "Relativistic-intensity near-single-cycle light waveforms at khz repetition rate," Light Science and Applications **9**, 47 (2020).
13. S. Kühn, M. Dumergue, S. Kahaly, S. Mondal, M. Füle, T. Csizmadia, B. Farkas, B. Major, Z. Várallyay, E. Cormier, M. Kalashnikov, F. Calegari, M. Devetta, F. Frassetto, E. Månsson, L. Poletto, S. Stagira, C. Vozzi, M. Nisoli, P. Rudawski, S. Maclot, F. Campi, H. Wikmark, C. L. Arnold, C. M. Heyl, P. Johnsson, A. L'Huillier, R. Lopez-Martens, S. Haessler, M. Bocoum, F. Boehle, A. Vernier, G. Iaquaniello, E. Skantzakis, N. Papadakis, C. Kalpouzos, P. Tzallas, F. Lépine, D. Charalambidis, K. Varjú, K. Osvay, and G. Sansone, "The ELI-ALPS facility: the next generation of attosecond sources," J. Phys. B: At., Mol. Opt. Phys. **50**(13), 132002 (2017).
14. R. Budriunas, T. Stanislauskas, J. Adamonis, A. Aleknavičius, G. Veitas, D. Gadonas, S. Balickas, A. Michailovas, and A. Varanavičius, "aaa," Opt. Express **25**(5), 5797–5806 (2017).
15. A. Vaupel, N. Bodnar, B. Webb, L. Shah, and M. C. Richardson, "Concepts, performance review, and prospects of table-top, few-cycle optical parametric chirped-pulse amplification," Opt. Eng. **53**(5), 051507 (2013).
16. D. Herrmann, L. Veisz, R. Tautz, F. Tavella, K. Schmid, V. Pervak, and F. Krausz, "Generation of sub-three-cycle, 16 tw light pulses by using noncollinear optical parametric chirped-pulse amplification," Opt. Lett. **34**(16), 2459–2461 (2009).
17. D. E. Rivas, A. Borot, D. E. Cardenas, G. Marcus, X. Gu, D. Herrmann, J. Xu, J. Tan, D. Kormin, G. Ma, W. Dallari, G. D. Tsakiris, I. B. Földes, S. w. Chou, M. Weidman, B. Bergues, T. Wittmann, H. Schröder, P. Tzallas, D. Charalambidis, O. Razskazovskaya, V. Pervak, F. Krausz, and L. Veisz, "Next generation driver for attosecond and laser-plasma physics," Sci. Rep. **7**(1), 5224 (2017).

Optics EXPRESS

18. S. Witte, R. T. Zinkstok, A. L. Wolf, W. Hogervorst, W. Ubachs, and K. S. E. Eikema, "A source of 2 terawatt, 2.7 cycle laser pulses based on noncollinear optical parametric chirped pulse amplification," Opt. Express **14**(18), 8168–8177 (2006).
19. O. Jahn, V. E. Leshchenko, P. Tzallas, A. Kessel, M. Krüger, A. Münzer, S. A. Trushin, G. D. Tsakiris, S. Kahaly, D. Kormin, L. Veisz, V. Pervak, F. Krausz, Z. Major, and S. Karsch, "Towards intense isolated attosecond pulses from relativistic surface high harmonics," Optica **6**(3), 280–287 (2019).
20. A. Kessel, V. E. Leshchenko, O. Jahn, M. Krüger, A. Münzer, A. Schwarz, V. Pervak, M. Trubetskov, S. A. Trushin, F. Krausz, Z. Major, and S. Karsch, "Relativistic few-cycle pulses with high contrast from picosecond-pumped opcpa," Optica **5**(4), 434–442 (2018).
21. F. Batysta, R. Antipenkov, J. Novák, J. T. Green, J. A. Naylon, J. Horáček, M. Horáček, Z. Hubka, R. Boge, T. Mazanec, B. Himmel, P. Bakule, and B. Rus, "Broadband opcpa system with 11 mj output at 1 khz, compressible to 12 fs," Opt. Express **24**(16), 17843–17848 (2016).
22. S. Prinz, M. Schnitzenbaumer, D. Potamianos, M. Schultze, S. Stark, M. Häfner, C. Y. Teisset, C. Wandt, K. Michel, R. Kienberger, B. Bernhardt, and T. Metzger, "Thin-disk pumped optical parametric chirped pulse amplifier delivering cep-stable multi-mj few-cycle pulses at 6 khz," Opt. Express **26**(2), 1108–1124 (2018).
23. B. Senfftleben, M. Kretschmar, A. Hoffmann, M. Sauppe, J. Tümmler, I. Will, T. Nagy, M. J. J. Vrakking, D. Rupp, and B. Schütte, "Highly nonlinear ionization of atoms induced by intense high-harmonic pulses," JPhys Photonics **2**(3), 034001 (2020).
24. R. Budriunas, T. Stanislauskas, and A. Varanavičius, "Passively CEP-stabilized frontend for few cycle terawatt OPCPA system," J. Opt. **17**(9), 094008 (2015).
25. P. Tournois, "Acousto-optic programmable dispersive filter for adaptive compensation of group delay time dispersion in laser systems," Opt. Commun. **140**(4-6), 245–249 (1997).
26. T. Nubbemeyer, M. Kaumanns, M. Ueffing, M. Gorjan, A. Alismail, H. Fattahi, J. Brons, O. Pronin, H. G. Barros, Z. Major, T. Metzger, D. Sutter, and F. Krausz, "1kw, 200mj picosecond thin-disk laser system," Opt. Lett. **42**(7), 1381–1384 (2017).
27. R. Jung, J. Tümmler, T. Nubbemeyer, and I. Will, "Thin-disk ring amplifier for high pulse energy," Opt. Express **24**(5), 4375–4381 (2016).
28. R. Jung, J. Tümmler, and I. Will, "Regenerative thin-disk amplifier for 300 mj pulse energy," Opt. Express **24**(2), 883–887 (2016).
29. M. Hübner, I. Will, J. Körner, J. Reiter, M. Lenski, J. Tümmler, J. Hein, B. Eppich, A. Ginolas, and P. Crump, "Novel high-power high repetition rate laser diode pump modules suitable for high-energy class laser facilities.," Instruments **3**(3), 34 (2019).
30. S. Prinz, M. Häfner, M. Schultze, C. Y. Teisset, R. Bessing, K. Michel, R. Kienberger, and T. Metzger, "Active pump-seed-pulse synchronization for opcpa with sub-2-fs residual timing jitter," Opt. Express **22**(25), 31050–31056 (2014).
31. T. Lang, A. Harth, J. Matyschok, T. Binhammer, M. Schultze, and U. Morgner, "Impact of temporal, spatial and cascaded effects on the pulse formation in ultra-broadband parametric amplifiers," Opt. Express **21**(1), 949–959 (2013).
32. J. Matyschok, T. Lang, T. Binhammer, O. Prochnow, S. Rausch, M. Schultze, A. Harth, P. Rudawski, C. L. Arnold, A. L'Huillier, and U. Morgner, "Temporal and spatial effects inside a compact and cep stabilized, few-cycle opcpa system at high repetition rates," Opt. Express **21**(24), 29656–29665 (2013).
33. B. Major, M. Kretschmar, O. Ghafur, A. Hoffmann, K. Kovacs, K. Varjú, B. Senfftleben, J. Tümmler, I. Will, T. Nagy, D. Rupp, M. J. J. Vrakking, V. Tosa, and B. Schütte, "Propagation-assisted generation of intense few-femtosecond high-harmonic pulses," JPhys Photonics **2**(3), 034002 (2020).
34. O. Hort, M. Albrecht, V. E. Nefedova, O. Finke, D. D. Mai, S. Reyné, F. Giambruno, F. Frassetto, L. Poletto, J. Andreasson, J. Gautier, S. Sebban, and J. Nejdl, "High-flux source of coherent xuv pulses for user applications," Opt. Express **27**(6), 8871–8883 (2019).
35. D. Rupp, N. Monserud, B. Langbehn, M. Sauppe, J. Zimmermann, Y. Ovcharenko, T. Möller, F. Frassetto, L. Poletto, A. Trabattoni, F. Calegari, M. Nisoli, K. Sander, C. Peltz, M. J. Vrakking, T. Fennel, and A. Rouzée, "Coherent diffractive imaging of single helium nanodroplets with a high harmonic generation source," Nat. Commun. **8**(1), 493 (2017).

94.134.197.137 {ts '2021-11-30 07:50:04'}